THE JOURNAL OF BIOLOGICAL CHEMISTRY
Vol. 274, No. 25, Issue of June 18, pp. 17869–17875, 1999
Printed in U.S.A.

Binding of Nucleotide Triphosphates to Cardiotoxin Analogue II from the Taiwan Cobra Venom (*Naja naja atra*)

ELUCIDATION OF THE STRUCTURAL INTERACTIONS IN THE dATP-CARDIOTOXIN ANALOGUE II COMPLEX*

(Received for publication, January 20, 1999, and in revised form, February 25, 1999)

Gurunathan Jayaraman, Thallampuranam Krishnaswamy Suresh Kumar, and Chin Yu‡

From the Department of Chemistry, National Tsing Hua University, Hsinchu, Taiwan, Republic of China

Snake venom cardiotoxins have been recently shown to block the enzymatic activity of phospholipid protein kinase and Na^+,K^+-ATPase. To understand the molecular basis for the inhibitory effects of cardiotoxin on the action of these enzymes, the nucleotide triphosphate binding ability of cardiotoxin analogue II (CTX II) from the Taiwan cobra (*Naja naja atra*) venom is investigated using a variety of spectroscopic techniques such as fluorescence, circular dichroism, and two-dimensional NMR. CTX II is found to bind to all the four nucleotide triphosphates (ATP, UTP, GTP, and CTP) with similar affinity. Detailed studies of the binding of dATP to CTX II indicated that the toxin molecule is significantly stabilized in the presence of the nucleotide. Molecular modeling, based on the NOEs observed for the dATP·CTX II complex, reveals that dATP binds to the CTX II molecule at the groove enclosed between the N- and C-terminal ends of the toxin molecule. Based on the results obtained in the present study, a molecular mechanism to account for the inhibition of the enzymatic activity of the phospholipid-sensitive protein kinase and Na^+,K^+-ATPase is also proposed.

Snake venom cardiotoxins are small molecular mass (~7 kDa), highly basic proteins cross-linked by four disulfide bridges (1–3). These toxins exhibit a wide variety of biological activities such as contraction of cardiac muscle cells, lysis of erythrocytes, and selective toxicity to certain types of tumor cells (4, 5). More recently, cardiotoxins have been demonstrated to selectively inhibit the action of certain key enzymes such as Na^+,K^+-ATPase and phospholipid-sensitive protein kinase (2, 6–8). Although the general molecular mechanism underlying the enzyme inhibitory action of cardiotoxins is still an enigma, it is contemplated that cardiotoxin could effectively block the enzymatic activities of Na^+,K^+-ATPase and phospholipid-sensitive protein kinase by competitively binding (in the present study) to adenosine triphosphate (ATP), which is a key substrate for the functioning of these enzymes. However, to date, the evidence for the binding of a nucleotide triphosphate to cardiotoxin has not been reported.

In the present study, for the first time, we demonstrate that the cardiotoxin analogue II (CTX II)[1] isolated from the Taiwan cobra venom (*Naja naja atra*) bind to nucleotide triphosphates. Herein, we also propose a molecular model of the CTX II·dATP complex and suggest a reasonable molecular mechanism to explain the reported inhibitory action of snake venom cardiotoxin on phospholipid-sensitive protein kinase and Na^+,K^+-ATPase.

MATERIALS AND METHODS

CTX II was purified as described by Yang *et al.* (9). The concentration of the protein was estimated from its absorbance at 280 nm ($\epsilon^{1\ mM}$ = 4.08). The nucleotides were purchased from Sigma. The concentration of the nucleotides was estimated (10) from their extinction coefficient values (ϵ^{259} = 15,400 for AMP, ADP, ATP, and dATP; ϵ^{271} = 9,000 for CTP; ϵ^{253} = 13,700 for GTP; and ϵ^{260} = 1,000 for UTP). All other chemicals used were of high quality analytical grade. All the experiments were performed at pH 3.0 and 25 °C unless otherwise mentioned.

Fluorescence Experiments—Fluorescence experiments were conducted on a Jasco HP 777 spectrofluorimeter. For tyrosine fluorescence, the excitation wavelength was set at 275 nm and the fluorescence was monitored at 310 nm. Both the excitation and emission slit widths were set at 5 nm in all the experiments.

Circular Dichroism Experiments—Circular dichroism measurements were made on a Jasco 720 spectropolarimeter. Cylindrical quartz cells of path length 0.1 and 1 mm were used for the measurements in the far (190~240 nm) and near (250~320 nm) UV regions. For thermal denaturation experiments, water-jacketed quartz cells were used and the temperature of the sample was controlled using a Neslab water bath.

NMR Experiments—The NMR experiments were performed on a Bruker DMX 600 MHz spectrometer. For all ^{1}H NMR titrations, the protein concentration used was 0.5 mM and for two-dimensional experiments 3 mM protein was used. The protein solutions were made using 50 mM glycine-d_5 (pH 3.0). For the purpose of assignment of individual proton resonances of the CTX II·dATP complex, TOCSY (11) and water-gated NOESY (12) spectra were recorded for appropriate molar ratio (as indicated under "Results and Discussion") of the CTX II-nucleotide in 95% H_2O, 5% D_2O. All spectra were obtained with 2048 complex data points in t_2 (detection period) and 512 points in t_1 (evolution period) with a spectral width of 7500 Hz. For hydrogen-deuterium exchange experiments, magnitude COSY spectra (2048 × 256 points) were recorded for the sample in 100% D_2O. Chemical shifts were calibrated against 3-(trimethylsilyl)propionate, sodium salt. The data were processed on an Indigo II workstation using the UXNMR software.

Calculation of Dissociation Constants—The dissociation constants (k_d) of the dATP and CTX II were calculated from the fluorescence intensity changes using the linear relation (13),

$$1/\Delta F = 1 + k_d/(L_o - \Delta F(C_o)) \quad \text{(Eq. 1)}$$

where ΔF is the change in the tyrosine fluorescence intensity upon addition of the nucleotide, L_o is the nucleotide concentration, and C_o is the concentration of the protein. The slope of the plot, $1/\Delta F$ *versus* $1/(L_o - \Delta F(C_o))$, yielded the dissociation constant value.

Molecular Modeling—The modeling of the CTX II·dATP complex was carried out in different steps. Minimizations were performed using the

* The work was supported by the National Science Council, Taiwan, and Dr. C. S. Tsou Memorial Medical Research Advancement Foundation grants. The costs of publication of this article were defrayed in part by the payment of page charges. This article must therefore be hereby marked "*advertisement*" in accordance with 18 U.S.C. Section 1734 solely to indicate this fact.

‡ To whom all correspondence should be addressed. Fax: 886-35-711082; E-mail: cyu@chem.nthu.edu.tw.

[1] The abbreviations used are: CTX II, cardiotoxin analogue II; NTP, nucleotide triphosphate.

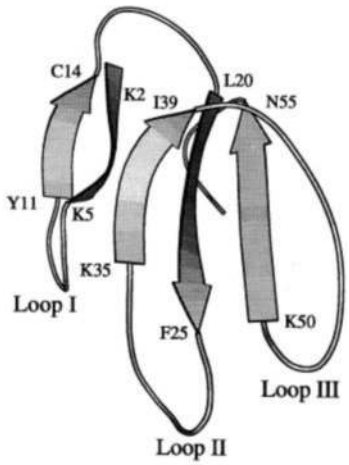

FIG. 1. **MOLSCRIPT representation of the backbone fold of CTX II.** Residues 2–5 and 11–14 form the antiparallel double-stranded β-sheet and residues 20–25, 34–39, and 50–55 form the antiparallel triple-stranded β-sheet segment.

CHARMm (14) energy function. The dATP molecule was built using the CHEMNOTE model building facility that is available within QUANTA (Molecular Simulations Inc.). The conformation of the adenine ring with respect to the deoxy sugar was set to be "anti." The molecule was then subjected to Powell energy minimization (500 steps) with the inclusion of the intramolecular NOE restraints that was available between the deoxyribose unit and the adenine moiety of dATP. The energy-minimized dATP molecule was then placed on the convex side of the CTX II (average solution structure; PDB entry code 1CRE). Both the dATP and the CTX II molecules were subjected to Adopted-Basis-Newton-Raphson energy minimization with the inclusion of the available intermolecular NOEs. Finally, with the inclusion of both intermolecular and the intramolecular NOEs (for CTX II and dATP), the entire complex was subjected to another few cycles of Adopted-Basis-Newton-Raphson energy minimization so as to obtain the lowest energy structure and avoid unnecessary bad contacts in the molecule. During this process the atomic restraints that had been imposed on the CTX II molecule were relaxed.

RESULTS AND DISCUSSION

Binding to NTPs—CTX II is a three-finger shaped (15, 16) protein (Fig. 1). The solution structure of the protein shows that the secondary structural elements in this toxin analogue include antiparallel double- and triple-stranded β-sheet segments (15, 16). In addition, CTX II is a class A protein as it lacks tryptophan residues and the aromatic amino acids in the toxin include three tyrosine residues (2). The binding affinity of the various nucleotide triphosphates (NTPs) to CTX II was investigated by monitoring the changes in the tyrosine fluorescence emission intensity at 310 nm as a function of the increasing concentrations of the various nucleotide triphosphates. The data presented in Fig. 2 depicts that all four nucleotide triphosphates (used in this study) cause a decrease in the emission intensity of CTX II, implying that all the four NTPs used could bind to protein (CTX II). The decrease in the 310 nm emission intensity might be due to the quenching effects of the NTPs bound to CTX II, at site(s) proximal to the tyrosine residues in the toxin molecule. The binding constants estimated from the tyrosine fluorescence decay curves are listed in Table I. Evaluation of the binding affinities (of different NTPs) to the protein from the calculated binding constant values (Table I) reveal that the binding affinity of all the four NTPs are in a similar range (16–32 μM). Thus, these results show that CTX II is a general NTP-binding protein.

To examine the influence of phosphate groups in the binding of NTPs to the CTX II molecule, we compared the binding affinities of ATP, ADP, AMP, and inorganic phosphate to CTX II. Addition of inorganic phosphate to the protein did not cause any significant change (data not shown) in the 310-nm emission even up to a concentration of 70 mM (10 times the concentration of the protein), implying that the changes in the emission intensity at 310 nm upon addition of the NTPs are due to the binding to the nucleoside portion of the NTPs used. Interestingly, the changes in the emission intensity at 310 nm upon addition of ATP, ADP, and AMP to CTX II reveal that all nucleotide derivatives used *per se* bind to the protein, but the binding avidity appears to be dependent on the length of the phosphate tail attached to the nucleoside. Thus, ATP with three phosphate groups shows the strongest binding (k_d = 15.69 μM, Fig. 2 and Table I) and AMP which possess one phosphate group shows the weakest (k_d = 87.36 μM, Fig. 2 and Table I) binding to CTX II. Hence, from the results of the experiments discussed above it is clear that CTX II binds to NTPs and the strength of the binding is strongly correlated to the length of the phosphate tail tethered to the nucleoside moiety. It should be mentioned that although CTX II appears to bind to all the four nucleotide triphosphates with similar affinity, for reasons of stability, we have used dATP as a model

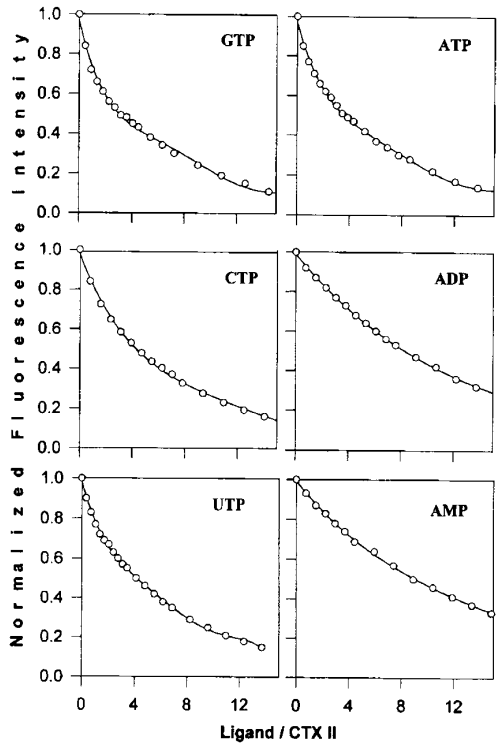

FIG. 2. **Changes in the tyrosine fluorescence intensity at 310 nm [λ_{ex} = 275 nm] shown as a function of nucleotide triphosphate(s) concentration.** The concentration of CTX II was 20 μM. The fluorescence intensity was normalized with respect to the native protein fluorescence.

TABLE I
The dissociation constant of different nucleotides calculated from the tyrosine fluorescence data, signifying the interaction between the nucleotides and the CTX II molecule

Nucleotide	Dissociation constant (k_d)
	μM
GTP	14.506
CTP	32.248
UTP	21.192
ATP	15.691
ADP	79.997
AMP	87.357
dATP	18.230

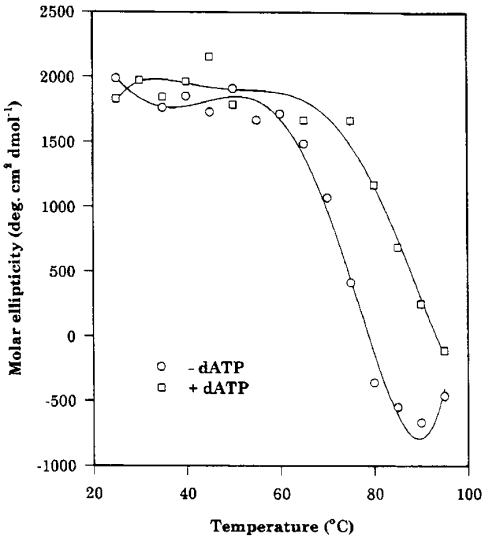

FIG. 3. **Changes in the ellipticity values (at 275 nm) of the dATP-bound (□) and free CTX II (○) as a function of temperature.** CTX II is found to unfold at 80 °C (T_m = 70 °C) in the absence of dATP whereas the unfolding of the protein is not complete even at 95 °C when it is bound to dATP.

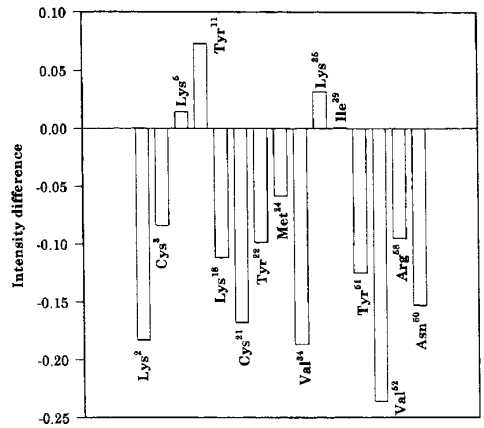

FIG. 4. **Difference in the (CαH-NH) cross-peak intensities as calculated from the magnitude COSY spectra recorded for the CTX II sample in the presence and absence of dATP (50 mM glycine-d_5 in 100% D_2O].** The intensities were normalized with respect to the intensities of the non-exchangeable aromatic protons. The data represents the difference(s) in the normalized intensity observed in free CTX II minus the normalized intensities in the dATP-bound CTX II.

NTP to understand the NTP-CTX II structural interactions in greater detail.

To probe if binding of NTP to CTX II is accompanied by conformational changes in the protein, the far and near UV-CD experiments were performed. Comparison of the far UV-CD spectra of the free CTX II and CTX II bound to dATP (in the molar ratio of 3:1 for dATP:CTX II) revealed no significant change in the 215 nm ellipticity values (representing the β-sheet secondary structural elements in the protein) was observed. These results thus indicate that binding of dATP to CTX II does not bring about any major change in the backbone folding of the protein but only causes minor perturbations in its side chain packing.

Effect of CTX II Stability upon Binding to dATP—To investigate the effect(s) of binding of dATP on the stability of the protein (CTX II), we compared the thermal stabilities of the CTX II in the free form and the dATP bound state by monitoring the change(s) in the 275-nm ellipticity as a function of increasing temperature. It was observed that the tertiary structural interactions in the protein (represented by the 275 nm ellipticity) show no change up to 60 °C but begins to melt rapidly beyond this temperature (Fig. 3). The unfolding process is complete at about 80 °C. Interestingly, the CTX II sample bound to dATP is resistant to denaturation even up to 75 °C (Fig. 3). It could be observed that the unfolding process is not complete even at a temperature of 95 °C (which is technically the maximum possible temperature we could perform the experiment). It is amply clear from the results of these experiments that binding of dATP to CTX II confers conformational stability to the protein.

Hydrogen-deuterium exchange detected by two-dimensional NMR technique is a facile and a sensitive technique to detect even subtle change(s) in the backbone of the protein, which sometimes could not be tracked by circular dichroism. Hence, we performed the hydrogen-deuterium exchange experiments to investigate for possible conformational alterations in CTX II upon binding to dATP (molar ratio 1:1). Magnitude COSY spectrum of free CTX II dissolved in D_2O (pD 3.4) showed that 27 cross-peaks (NH, CαH) are protected from exchange in the native state of the protein (data not shown). This probably implies that these 27 amide protons are either involved in hydrogen bonding or the corresponding amide protons are located in the protein interior. In comparison, magnitude COSY spectrum (data not shown) of CTX II bound to dATP also showed the same number of 27 cross-peaks (NH, CαH) in the fingerprint region. Thus, it appears that there is/are no drastic conformational change(s) in the backbone of the protein upon binding to dATP. Although the number of (NH, CαH) cross-peaks of the free and the bound forms are the same, it is also important to compare the relative cross-peak (NH, CαH) intensities in the magnitude COSY spectra representing the free and the dATP bound form of CTX II (Fig. 4). Comparison of the relative cross-peak intensities of the 27 protected amide protons in the native and dATP bound forms of CTX II (Fig. 4) reveal that several residues in the dATP bound form show higher protection against exchange than when the protein is not bound to dATP. The residues showing relatively higher protection against exchange include Lys^2, Cys^3, Lys^{18}, Cys^{21}, Tyr^{22}, Met^{24}, Val^{34}, Tyr^{51}, Val^{52}, Arg^{58}, and Asn^{60}. Interestingly, most of these residues depicting higher protection (in the dATP bound state of CTX II) are located in the β-strands III, IV, and V and in the N- and C-terminal ends of the CTX II molecule. Thus, the results of the hydrogen-deuterium exchange experiments not only give useful clues regarding the dATP-binding site on the protein but also unambiguously demonstrate that binding of dATP to the protein (CTX II) stabilizes the structure of the protein.

As the results of the experiments described thus far demonstrate that dATP binds to CTX II, it would be interesting to probe the location of the dATP-binding site on the three-dimensional structure of the protein. In this context, we employed one- and two-dimensional NMR spectroscopy.

Location of dATP-binding Site—One-dimensional NMR experiments provide an idea of the site(s) of interaction(s) of the ligand on the protein. These experiments provide clear information on the chemical environment at the ligand interaction site(s) on the protein. In general, protein-ligand interactions using one-dimensional NMR spectroscopy could be discerned from the changes in the 1) broadening effects in the line width of the individual proton resonance(s) and/or from 2) the relative chemical shift difference(s) between the free and bound form of the protein. In this context, a series of one-dimensional NMR spectra (Fig. 5) were recorded (at 25 °C) at varying dATP:CTX II ratios (0–1.5). The chemical shift values of many proton

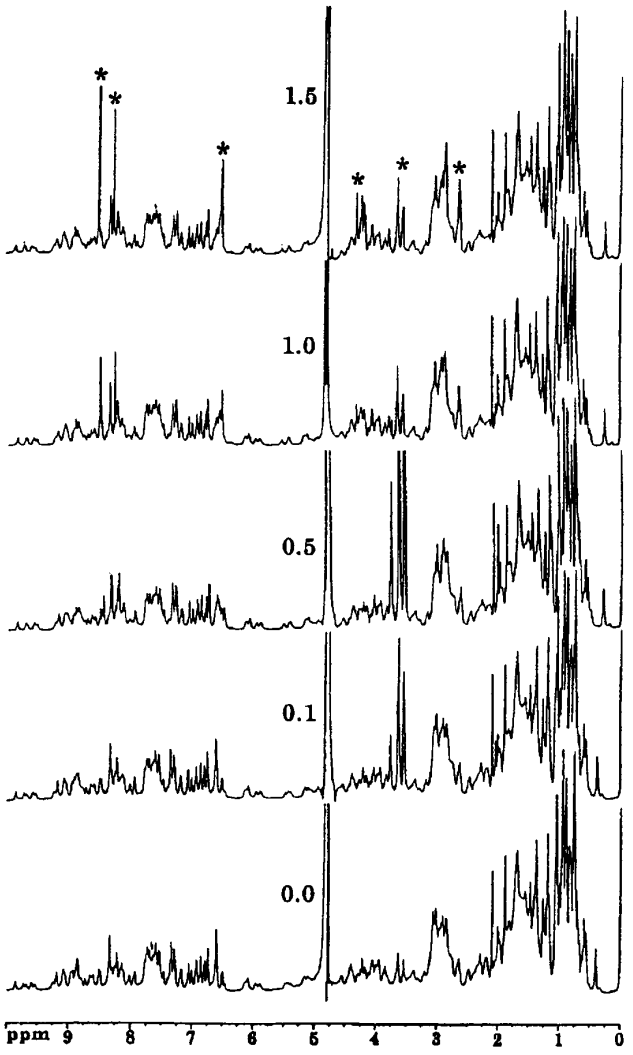

FIG. 5. **One-dimensional NMR spectra of CTX II in the absence and presence of dATP.** The numbers (near the water signal) represent the molar ratio of dATP to CTX II. All spectra were recorded in 50 mM glycine-d_5 (pH 3.0) at 25 °C. The chemical shifts were referenced to 3-(trimethylsilyl)propionate, sodium salt. The *asterisks* on selected proton resonance signals indicate those that arise from dATP.

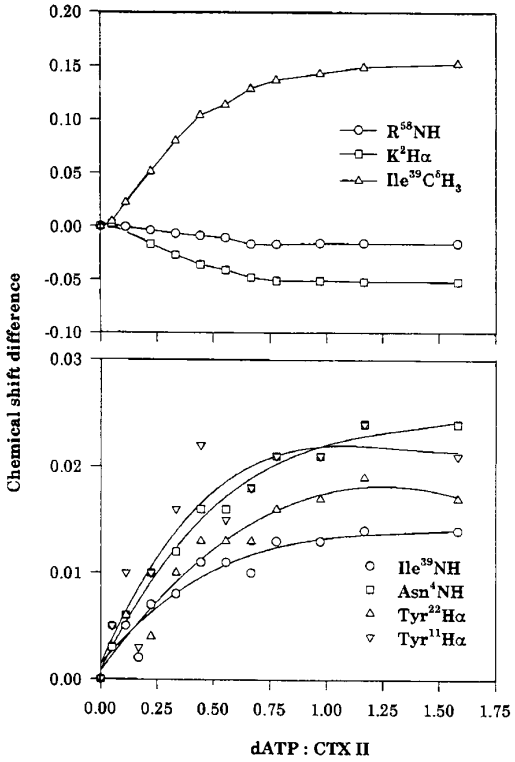

FIG. 6. **Changes in the chemical shift of selected, isolated proton resonances as detected from the one-dimensional proton NMR spectra, as a function of molar ratio of dATP to CTX II.** The changes in the observed chemical shift values are found to saturate at a dATP to CTX II molar ratio of 1:1.

resonances, in the presence of dATP showed significant differences as compared with the free form of the protein. Only the changes accompanying a few selected non-overlapping resonances could be unambiguously followed at increasing molar ratios of dATP:CTX II. The titration curves evaluated as a function of the molar ratio(s) of dATP:CTX II are hyperbolic and tend to saturate when the dATP:CTX II molar ratio reaches a value close to one (Fig. 6). This aspect apparently suggests a 1:1 binding of the nucleotide triphosphate to the protein (Fig. 6). A close examination of the chemical shift values of the various proton resonances (which could be unambiguously monitored in one-dimensional spectrum) reveals that the amide proton resonances of Ile^{39}, Asn^{4}, and Arg^{58} undergo the most pronounced drift in the chemical shift values (Fig. 6). It is interesting to note that Asn^{4} and Arg^{58} are located at the terminal ends of the cardiotoxin molecule. Incidentally, the solution structure of the free-form of CTX II reveals that the N- and C-terminal ends of the CTX II molecule are in close proximity tethered together by hydrogen bonds among their backbone atoms (15, 16). In this context, it is probable that dATP binds to CTX II at region(s) where the N- and C-terminal ends of the molecule are bridged together. In addition to the amide proton of Ile^{39}, the side chain methyl proton ($Ile^{39}C^{\delta}H_3$) also exhibited reasonably significant upfield shift (Fig. 6). Ile^{39}, which is a part of the triple-stranded β-sheet segment is located at a site which is spatially 10 Å from the N and C termini of the CTX II molecule. Although this residue (Ile^{39}) is located at a position well separated from the putative dATP-binding site, the observed large magnitude drift could be possibly due to the small local destabilization of the native structural interactions at the dATP-binding site. Such a subtle molecular reorganization in the protein molecule, upon binding to dATP, possibly brings the isoleucine terminal methyl group spatially closer to the conserved phenolic ring of Tyr^{22} (whose aromatic ring is spatially close to Ile^{39} in the native three-dimensional structure of CTX II). In such an event, the terminal methyl group is expected to experience larger ring current effects (compared with native) leading to the observed change in the chemical shift values for the methyl group protons. In addition, to the amide protons and the side chain methyl group(s), the α-proton ($C\alpha H$) resonances of a few residues (which could be monitored) also showed significant differences in the chemical shift values upon binding to the nucleotide (Fig. 6). The changes in the $C\alpha H$ chemical shift values of Tyr^{11}, Tyr^{22}, and Lys^{2} are remarkable. Lys^{2} is located in the double-stranded β-sheet segment and as stated earlier plays a key role in bridging the N and C termini (16). Tyrosine residues located at positions 11 and 22 are lodged in the double- and triple-stranded β-sheet segments, respectively. Tyr^{22} is one of the most well conserved residue found in all the cardiotoxin isoforms (17–19). This residue (Tyr^{22}) is the locus of a prominent hydrophobic core that plays an important role in maintaining the structural integrity of the three-dimensional structure of cardiotoxins. Chemical modification of Tyr^{22} has been reported to result in drastic disruption of tertiary structural interactions, rendering the toxin molecule

inactive (20). In addition, a comparison of the three-dimensional solution structures of various cardiotoxin isoforms isolated from Taiwan cobra (*Naja naja atra*) venom shows that the aromatic rings of Tyr^{22} and Tyr^{51} lie parallel to one another (2). It appears that local destabilization effects at the dATP-binding site (upon binding to dATP) in the protein are effectively transmitted to residues which are spatially far away from the putative binding site accounting for the observed change(s) in the chemical shift values of some of the protons of residues (spatially separated from the dATP-binding site). The local perturbation occurring upon binding to dATP (at the contemplated dATP binding site) appears to force the Ile^{39} side chain atoms to move closer to the aromatic ring of Tyr^{22}. It appears that the mobility of a bulky hydrophobic side chain (Ile^{39}) further influences the native molecular interactions stabilizing the phenolic ring of Tyr^{22}. Since the aromatic rings of Tyr^{22} and Tyr^{51} are spatially juxtaposed, the subtle destabilization effects are probably further transmitted to Tyr^{51}. Our proposal of this molecular "destabilization relay" is supported by the observed chemical shift changes of the amide protons of the residues involved in the above mentioned destabilization relay. The slight decrease in the ellipticity value at 270 nm in the near UV-CD experiment, upon protein binding to dATP supports our contention that the native aromatic interactions (contributing to the CD signal) are affected upon the protein molecule binding to dATP. Ubbink and Bendall (21) recently characterized the plastocyanic-cytochrome *c* complex. The authors observed changes in chemical shifts of those protons, which are spatially far away from the binding site. This phenomenon is attributed to arise from the "secondary effects" resulting from the complex formation. Similarly, the chemical shifts observed in the present study could be due to such secondary effects (by destabilization relay). Estimation of the association constant values from the proton chemical shifts reveal that dATP binds to the CTX II molecule with a binding constant value in the micromolar range which is *in par* with those obtained from the fluorescence experiment(s). Thus, from the results obtained from the one-dimensional NMR experiments, it appears that dATP binds specifically with CTX II and the interacting site is contemplated to be located in the cleft formed between the N- and C-terminal ends of the molecule.

To obtain complete insight of the structural interactions stabilizing the dATP·CTX II complex, two-dimensional NMR experiments (22) were carried out (at 1:1 molar ratio of dATP:CTX II). Most of the proton resonances pertaining to dATP, free CTX II, and dATP bound to CTX II were assigned unambiguously using the TOCSY and NOESY spectra. Analysis of the spectral data of the two-dimensional NMR experiments revealed that the chemical shift values of many protons in the protein (in the free form) had significantly changed upon interaction with dATP. Some of these changes could be monitored only from the two-dimensional NMR data because of the overlap of the resonances in the one-dimensional ^1H NMR spectra discussed earlier. There are several protons of the protein backbone which show significant differences (>0.02 ppm) in the chemical shift upon complexation. These include the amide and/or α-protons of Lys^2, Asn^4, Lys^5, Val^7, Tyr^{11}, Tyr^{22}, Lys^{23}, Met^{24}, Arg^{36}, Cys^{38}, Ile^{39}, Val^{41}, Lys^{44}, Ser^{46}, Tyr^{51}, Cys^{53}, and Arg^{58} (data not shown). Interestingly, most of the residues showing appreciable change(s) in their chemical shift values after binding to dATP are located in the N- and C-terminal ends and β-strands III and IV of the CTX II molecule. It should be mentioned that the differences observed in the amide and the α-protons of few residues that are situated topologically at site(s) far away from the contemplated nucleotide-binding site could possibly be due to minor secondary conformational effects. It should be of interest to note that the backbone amide protons (of tyrosine residues) show significant differences in their chemical shift values upon binding to dATP (data not shown). This feature strongly suggests that the three tyrosine residues are located near or in the nucleotide-binding site on the protein. Similar conclusions were reached from the results of the tyrosine fluorescence experiments and the one-dimensional NMR experiments as discussed earlier. Clinching evidence for protein-ligand interaction(s) based on two-dimensional NMR experiments comes from the observation of intermolecular NOEs between the protons of the ligand and that of the protein. Analysis of the NOEs obtained in the NOESY spectrum of the dATP·CTX II complex shows that there are at least 11 unambiguous intermolecular NOEs characterizing the complex between the nucleotide and the protein (Table II). Several of the observed intermolecular NOEs are with the sugar moiety of dATP. Prominent among the intermolecular NOEs signifying the protein-dATP interaction include Lys^2NH-H2′, $Ile^{39}C\delta H_3$-H2′, $Ile^{39}C\delta H_3$-H2″, and Asp^{57}NH-H4′ (Fig. 7). The $Leu^1H\alpha$-H8 symbolizes the sole intermolecular NOE characterizing the protein-adenine ring interaction(s). In addition, several other NOEs are observed for the protein-sugar interaction (Table II).

TABLE II
List of intermolecular NOEs observed in the NOESY spectrum (250 ms) of the CTX II·dATP (1:1) complex (50 mM glycine, pH 3.0, 25 °C)

CTX II	dATP	NOE intensity
Leu^1-Hα	H8	Very weak
Leu^1-Hα	H4′	Medium weak
Lys^2-HN	H2′	Medium weak
Lys^2-HN	H2′	Medium weak
Cys^3-Hβ′	H4′	Very weak
Ile^{39}-Hδ	H2′	Medium
Ile^{39}-Hδ	H2″	Medium
Thr^{56}-$C^{\gamma}H_3$	H4′	Medium
Asp^{57}-HN	H4′	Medium
Cys^{59}-Hβ′	H4′	Weak
Cys^{59}-Hβ″	H4′	Weak

It is important to address the question as to why only one intermolecular NOE represents the protein-adenine ring interaction. In this context, it is important to compare the amino acid sequences of well known nucleotide-binding proteins and that of CTX II. Kabsch and Holmes (23) upon detailed search for the consensus nucleotide binding motif among the proteins in the data bank, reported that the amino acid sequence, (Ile/Leu/Val)-*X*-(Ile/Leu/Val/Cys)-Asp-*X*-Gly-(Thr/Ser/Gly)-(Thr/Ser/Gly)-*X*-*X*-(Arg/Lys/Cys), represents the nucleotide binding motif. The amino acid sequence of CTX II interestingly revealed the presence of a nucleotide binding sequence, Val^{32}-Pro^{33}-Val^{34}-Lys^{35}-Arg^{36}-Gly^{37}-Cys^{38}-Ile^{39}-Asp^{40}-Val^{41}-Cys^{42}. It could be discerned that the CTX II shares more than 80% amino acid sequence homology with the reported consensus nucleotide binding motif. A closer look at the nucleotide binding motif in CTX II shows the absence of a crucial, non-variant aspartic acid present in the amino acid sequences of all the nucleotide-binding proteins known so far (23). The charged carboxylate group of aspartic acid is believed to stabilize the adenine ring through a hydrogen bond with the amino group located in the purine ring (23). A positively charged lysine residue in CTX II replaces the conserved aspartic acid. It is possible that the positive charge on lysine does not produce similar stabilization (due to charge incompatibility or electrostatic repulsion(s)) of the dATP molecule. This renders greater mobility for the adenine ring accounting for the absence of the expected intermolecular NOEs with the protein molecule.

Conformation of dATP—It is pertinent to address the question of the spatial orientation of the adenine ring with respect

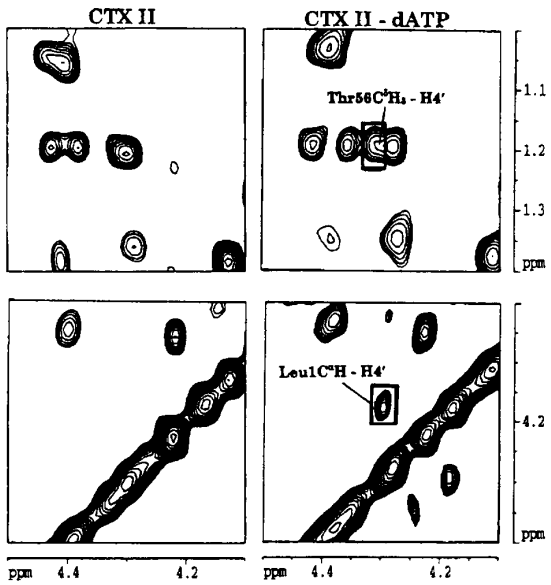

FIG. 7. **NOE cross-peaks that are observed between the CTX II and the dATP molecule in the NOESY spectra recorded with a mixing period of 250 ms.** The NOEs in the NOESY spectra of free CTX II is shown for comparison.

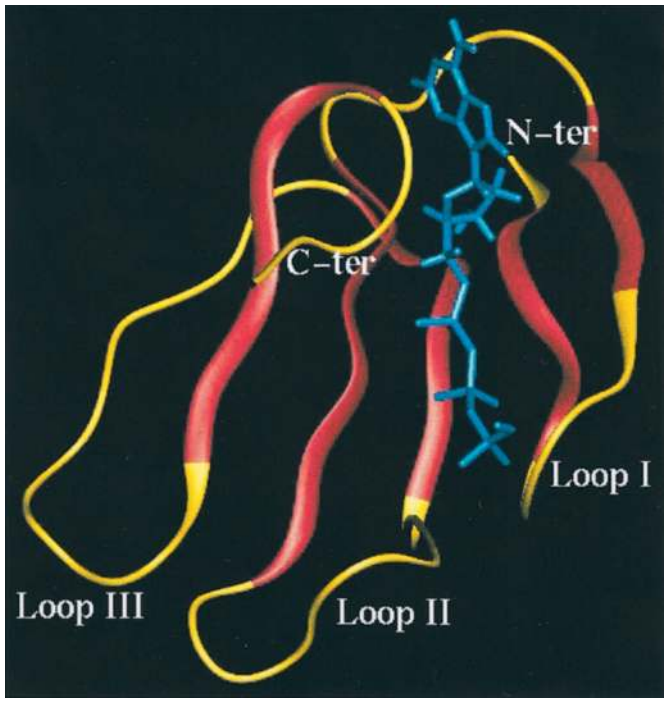

FIG. 8. **Graphical representation of the dATP molecule interacting with CTX II.** The dATP molecule could be seen to be lodged in the groove between the N- and C-terminal ends of the CTX II molecule.

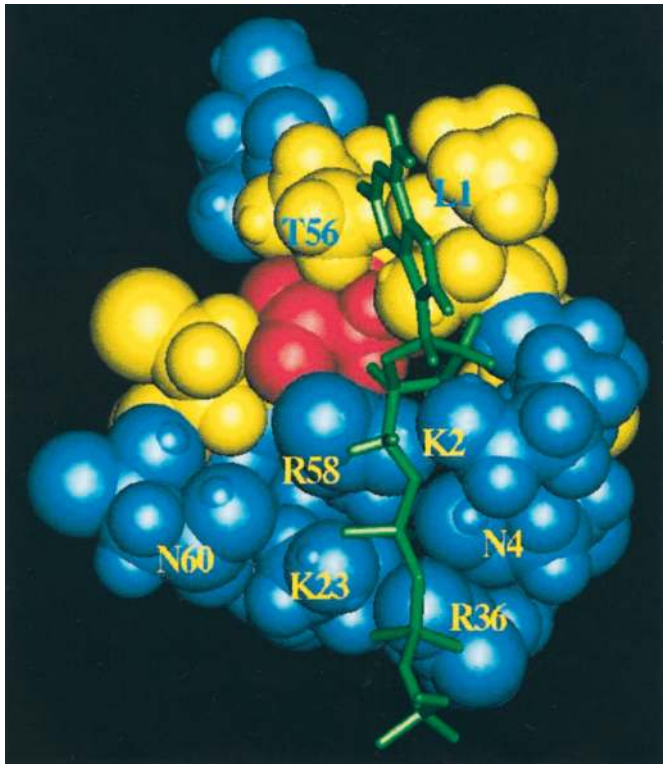

FIG. 9. **Molecular model of the CTX II·dATP complex.** The nucleotide could be seen to lodge in between the the N- and C-terminal end of the CTX II molecule. It is also evident that the negatively charged pyrophosphate group of the dATP segment is stabilized by the electrostatic interactions with the positively charged lysines and arginines of CTX II. The dATP molecule is shown in *green*.

to the deoxyribose sugar in the dATP molecule bound to the protein. It is well known that the nucleotides in the unbound or free form adopt a *syn* conformation (24). Upon binding to macromolecules, the nucleotides exist in either *anti* or *syn* conformation (25). The conformation of the bound nucleotide is considered to be *syn*, if the intramolecular NOEs (in the dATP molecule) between the H2 proton in the adenine ring and H2′, H2′′, H3′, and H5′ protons in sugar moiety (24, 26) are observed. On the contrary, if one detects NOEs between the H8 proton (of the adenine ring) and H1′, H2′, H4′, and H5′ of the sugar ring, the conformation of the bound nucleotide could be termed to be *anti*. A critical examination of the observed intramolecular NOEs between the sugar and the adenine ring (in the dATP molecule bound to CTX II) shows that intramolecular NOEs (between H8 proton of the adenine ring and the H1′, H2′, H2′′, H4′ of the deoxy ribose sugar) are quite similar to that expected for the *anti* conformation (of the nucleotide). Therefore, dATP adopts *anti* conformation upon binding to the CTX II molecule.

Molecular Modeling of CTX II·dATP Complex—Molecular modeling of the CTX II-dATP interaction was attempted to obtain a visual concept of the topology of the dATP-binding site and the structural interactions in operation at the nucleotide triphosphate-CTX II interface. The proposed model of the CTX II·dATP complex is in good agreement with the experimental NMR data. Interestingly, the total CHARMm energy of the free form of CTX II (-675 kcal mol^{-1}) was lower than that of the dATP bound form of the protein (-781 kcal mol^{-1}). This further implies that CTX II gains extra stabilization upon binding to the nucleotide triphosphate. This result is in conformity with the conclusions drawn from the results of the thermal denaturation and hydrogen-deuterium exchange experiments. The structure of the dATP·CTX II complex depicts the dATP molecule lodged in the groove enclosed by the N- and C-terminal ends of the molecule (Fig. 8). The energy minimized structure reveals that the protein-dATP complex is stabilized by a variety of electrostatic interactions. The negatively charged triphosphate moiety of the dATP molecule is found to strongly interact with the "cationic cluster" at the terminal ends (N and C termini). The residues in the cationic cluster interacting with the triphosphate moiety are Lys^{2}, Asn^{4}, Arg^{36}, and Arg^{58} (Fig. 9). It is interesting to note that among the three phosphate groups in dATP, the oxygen atoms of the α- and β-phosphate groups are spatially closer to the residues comprising the cat-

ionic cluster. The negatively charged oxygen atom of the γ-phosphate group, interestingly, does not possess any significant interaction(s) with the cationic residues in the protein. It appears that the phosphate groups in the α and β positions of the nucleotide triphosphate dictates the binding efficiency of the ligand molecule to the cationic cluster spread on the cardiotoxin molecule. The negatively charged phosphate groups of the dATP molecule are placed across the middle of Loop II of the CTX II molecule (Fig. 9). Such a topological location brings the negatively charged phosphate groups of dATP spatially closer to some of the residues located in Loop I. For example, the aromatic residue, Tyr^{11}, located in Loop I is found to be located at a spatial distance of 6 Å from the β-phosphate group of dATP. Due to the proximity of the phenolic ring (of Tyr^{11}) to the negatively charged β-phosphate, it is possible that the aromatic ring experiences an electrostatic repulsion leading to minor perturbations in the native interactions in this portion of the molecule. Interestingly, the change in the chemical shift values of the amide protons of Tyr^{11} appears to support our contention. In addition to the phosphate group(s)-mediated interactions, the energy minimized CTX II·dATP complex structure also reveals additional interactions between dATP and the protein. The hydroxyl groups of the deoxy sugar are found to interact with the protein through the amide groups (of the backbone) contributed by the amino acid residues located at the N- and C-terminal ends such as Lys^2, Cys^3, Asp^{57}, and Cys^{59}.

Go and co-workers (27) recently analyzed the structural features of the nucleotide-binding site in various proteins, which have strong propensity to bind to nucleotides. Based on a thorough search, it was found that the nucleotide-binding site is normally located in the "charged sockets" comprising of cationic residues. In general these charged sockets are found to be located at a topological site wherein the N- and C-terminal ends of the protein come close to one another. In addition, this study revealed that at the site(s) closer to the nucleotide-binding site, the backbone of the protein to have strong propensity to adopt β-sheet conformation. Interestingly, the ATP-binding site in CTX II exhibits structural features quite similar to that of the consensus nucleotide-binding site.

Implications of CTX II-dATP Interaction—Cardiotoxins as stated earlier are bestowed with a broad range of biological properties (2). Recently, cardiotoxins isolated from various snake venom sources have been demonstrated *in vitro* to competitively inhibit the enzymatic activity of phospholipid-sensitive (Ca^{2+} dependent) protein kinase and activated Na^+,K^+-ATPase bound to the erythrocyte membrane and muscle cells (6–8). It is interesting to note that both these enzymes are membrane bound and binding to ATP is obligatory for their enzymatic activity. Cardiotoxins are membrane active proteins (2) and are known to bind and penetrate through the membrane and also possess the ability to strongly bind to nucleotide triphosphates (including ATP as reported in the present study). Thus, it appears that CTX II due to its nucleotide triphosphate binding ability, probably competes with these ATP-dependent enzymes for binding to ATP leading to the effective inhibition of the catalytic action of these enzymes. It is interesting to note that the binding constant of dATP to CTX II is in the same range as that of phospholipid-sensitive protein kinase (~30 μM) (28) and Na^+,K^+-ATPase (124 μM) (29). This supports our viewpoint that the snake venom cardiotoxin block the enzymatic action of these two enzymes by sequestering the ATP and inhibit the biological activities of protein kinase and Na^+,K^+-ATPase.

The present study is the first report wherein the binding of nucleotide triphosphates, including ATP, has been presented for a snake venom cardiotoxin. This finding, in our opinion, implicates the role of cardiotoxins in the control of many cellular processes. It is believed that more detailed studies exploring the significance of binding of the nucleotide triphosphates to snake venom cardiotoxins would be conducted in the near future.

Acknowledgment—We acknowledge the Regional Instrumentation Center, Hsinchu, Taiwan for allowing us to use the 600 MHz NMR spectrometer facility.

REFERENCES

1. Harvey, A. L. (1983) *J. Toxicol. Toxin Rev.* **4,** 41–69
2. Kumar, T. K. S., Jayaraman, G., Lee, C. S., Arunkumar, A. I., Sivaraman, T., Samuel, D., and Yu, C. (1997) *J. Biomol. Struct. Dyn.* **15,** 431–463
3. Kumar, T. K. S., Pandian, S. K., and Sailam, S. (1998) *J. Toxicol. Toxin. Rev.* **17,** 183–212
4. Kumar, T. K. S., Pandian, S. K., Jayaraman, G., and Yu, C. (1999) *Proc. Natl. Sci. Council Repub. China,* **23,** 1–19
5. Kumar, T. K. S., Lee, C. S., and Yu, C. (1996) in *Natural Toxins* (Singh, B. R., and Tu, A. T., eds) pp. 114–129, Plenum Press, New York
6. Kuo, J. F., Raynor, R. L., Mazzei, Schatzman, R. S. Turner, R. S., and Kem, W. R. (1983) *FEBS Lett.* **153,** 183–186
7. Raynor, R. L., Zheng, B., and Kuo, J. F. (1991) *J. Biol. Chem.* **266,** 2753–2758
8. Chiou, S. H., Raynor, R. L., Zheng, B., Chambers, T. C., and Kuo, J. F. (1993) *Biochemistry* **32,** 2062–2067
9. Yang, C. C., King, K., and Sun, T. P. (1981) *Toxicon* **19,** 645–649
10. Sambrook, J., Fritsch, E. F., and Maniatis, T. (1989) in *Molecular Cloning: A Laboratory Manual* (Nolan, C., ed) Cold Spring Harbor Laboratory Press, Cold Spring Harbor, NY
11. Bax, A., and Davies, D. G. (1985) *J. Magn. Res.* **65,** 355–360
12. Piotto, M., Sandek, V., and Skelnar, V. (1992) *J. Biomol. NMR.* **2,** 661–665
13. De Macro, A., Petros, A. M., Laursen, R. A., and Llinas, M. (1987) *Eur. Biophys. J.* **14,** 359–368
14. Brooks, B. R., Bruccoleri, R. E., Olafson, S. D., States, D. J., Swaminathan, S., and Karplus, M. (1983) *J. Comput. Chem.* **4,** 187–217
15. Bhaskaran, R., Huang, C. C., Tsai, Y. C., Jayaraman, G., Chang, D. K., and Yu, C. (1994) *J. Biol. Chem.* **269,** 23500–23508
16. Jang, J. Y., Kumar, T. K. S., Jayaraman, G., Yang, P. W., and Yu, C. (1997) *Biochemistry* **36,** 14635–14641
17. Lee, C. S., Kumar, T. K. S., Lian, L.-Y., Cheng, J. W., and Yu, C. (1998) *Biochemistry* **37,** 155–164
18. Sivaraman, T., Kumar, T. K. S., Chang, D. K., Lin, W. Y., and Yu, C. (1998) *J. Biol. Chem.* **273,** 10181–10189
19. Bhaskaran, R., Huang, C. C., Chang, D. K., and Yu, C. (1994) *J. Mol. Biol.* **235,** 1291–1301
20. Roumestand, C., Gilquin, B., Tremeau, O., Gatineau, E., Mouawad, L., Menez, A., and Toma, F. (1994) *J. Mol. Biol.* **243,** 719–735
21. Ubbink, M., and Bendall, D. S. (1997) *Biochemistry* **36,** 6326–6335
22. Wuthrich, K. (1986) *NMR of Proteins and Nucleic Acids,* John Wiley and Sons Inc., New York
23. Kabsch, W., and Holmes, K. C. (1995) *FASEB J.* **9,** 167–174
24. Garin, J., Vignais, P. V., Gronenborn, A. M., Clore, G. M., Gao, Z., and Bauerlein, E. (1988) *FEBS Lett.* **242,** 172–182
25. Grishan, C. M. (1988) *Methods Enzymol.* **156,** 353–371
26. Traut, T. W. (1994) *Eur. J. Biochem.* **222,** 9–19
27. Kobayashi, N., and Go, N. (1997) *Nat. Struct. Biol.* **4,** 6–7
28. Whitehouse, S., Feramisco, J. R., Casnellie, J. E., Krebs, E. G., and Walsh, D. A. (1983) *J. Biol. Chem.* **258,** 3693–3701
29. Lin Shiau, S. Y., Huang, M. C., and Lee, C. Y. (1976) *J. Pharmacol. Exp. Ther.* **196,** 758–770